SCIENCE CHINA
Information Sciences

• REVIEW •
Special Focus on Quantum Information

August 2020, Vol. 63 180502:1–180502:19
https://doi.org/10.1007/s11432-020-2932-8

Superconducting X-ray detectors

Can YANG[1,3], Mengting SI[1,3] & Lixing YOU[1,2,3,4*]

[1] *State Key Laboratory of Functional Materials for Informatics, Shanghai Institute of Microsystem and Information Technology (SIMIT), Chinese Academy of Sciences, Shanghai* 200050*, China;*
[2] *Center of Materials Science and Optoelectronics Engineering, University of Chinese Academy of Sciences, Beijing* 100049*, China;*
[3] *CAS Center for Excellence in Superconducting Electronics (CENSE), Shanghai* 200050*, China;*
[4] *Zhejiang Photon Technology Co. Ltd., Guigu Science Park, Jiashan* 314100*, China*

Received 12 February 2020/Revised 20 April 2020/Accepted 20 May 2020/Published online 15 July 2020

Abstract Owing to their high sensitivity and low noise, superconducting detectors are used for photon detection from microwave to high-energy particles. X-ray detection plays an important role in materials analysis, astronomy, and medical radiography, which require high efficiency as well as high energy resolution. However, traditional semiconducting detectors cannot fulfill these requirements. In this article, we review superconducting quantum detectors for X-ray detection, including transition-edge sensor (TES), superconducting tunneling junctions (STJs), kinetic inductance detectors (KIDs) and superconducting nanowire single-photon detectors (SNSPDs), and introduce the physical structures, working mechanisms, and device behaviors of these detectors. We also review their performances regarding X-ray detection and analyze their respective characteristics. According to recent progress and the requirements of various applications, possible improvement of superconducting detectors for X-rays are discussed.

Keywords superconducting X-ray detectors, transition-edge sensors, superconducting tunneling junctions, kinetic inductance detectors, superconducting nanowire single-photon detector

Citation Yang C, Si M T, You L X. Superconducting X-ray detectors. Sci China Inf Sci, 2020, 63(8): 180502, https://doi.org/10.1007/s11432-020-2932-8

1 Introduction

1.1 Requirements of X-ray detection

Since its discovery by Wilhelm Rontgen, X-ray has been used in various fields of research [1]. Up until now, X-ray detection has played an important role in materials analysis [2], security inspection [3], X-ray astronomy [4], and medical radiography [5]. X-ray detection has various respective needs. For materials analysis and X-ray astronomy, high energy and spatial resolution over a relatively large field of view are necessary. In contrast, both security inspection and medical radiography require a quick response and high sensitivity for security reasons, and high quantum efficiency is in demand for all applications.

There are four different types of X-ray detectors: gas-filled detectors, scintillation detectors, semiconducting detectors [6] and superconducting detectors. The most frequently used hypersensitive detectors are semiconducting detectors and superconducting detectors. The mainstream semiconducting detector for X-ray detection is the silicon drift detectors (SDDs). SDDs are based on the principle of sideward depletion introduced in the study by Gatti and Rehak in 1984 [7]. They can combine a large sensitive area with a small value of the output capacitance and are suited for high count rate X-ray spectroscopy [8]. However, the energy resolution of SDDs is limited to 130 eV [9] because of their relatively large bandgap,

* Corresponding author (email: lxyou@mail.sim.ac.cn)

which is gradually dissatisfied the needs in some soft X-ray detection, such as materials analysis and astronomy. In recent years, perovskites scintillators served as absorbers have been proved to have good performance in medical radiography [10]. Compared with semiconducting X-ray detectors, superconducting X-ray detectors perform better (high energy resolution $\Delta E/E \sim 10^{-3}$, single photon detection, and high counting efficiency) owing to the suppression of thermal noise at a low operating temperature and the presence of small energy gaps, and have become increasingly popular, along with the development of cryogenic technology.

1.2 Physics of superconducting detectors

Superconductors are different from other materials owing to zero DC resistance, a perfect diamagnetism (Meissner effect) and macroscopic quantum phenomena below critical temperature [11–13]. Many superconducting applications are related to these three properties. The zero DC resistance characteristic was discovered by Kamerlingh Onnes in 1911, and has been applied to transmit and store energy to reduce energy dissipation [14], and produce high magnetic fields with a large current [15]. Meissner effect has been used to shield magnetic field [16]. Macroscopic quantum effects, including Josephson effect and fluxoid quantization, arise from the quantum interference of the superconducting electron state. Macroscopic quantum effects of superconductors have many applications pertaining to sensors, detectors, and circuits, such as superconducting quantum interference devices (SQUIDs), single flux quantum (SFQ), and quantum computing [17]. Regarding superconducting detectors in this review, they possess single-photon response characteristics, so they can be regarding as quantum-counting counters. When superconducting detectors absorb a single photon, there will appear a high-energy electron, which will result in an exponential growth of low-energy nonequilibrium electrons in time by electron-electron and electron-phonon interaction. The maximum number of nonequilibrium electrons is referred as quantum yield [18]. Meanwhile, superconducting detectors possess extremely high sensitivity closing to quantum limit.

Regarding superconductors, two related electrons are bound together, and the binding energy prevents them from scattering, which allows them to flow without resistance. In traditional BCS superconductors, this phenomenon has been explained by microscopic and macroscopic theories since the 1950s [19, 20]. Almost at the same time, transition-edge sensor (TES) was first developed to detect photons [21, 22]. In microscopic BCS theory, the interaction distance of the two electrons in a Cooper pair is described by the temperature-dependent coherent length $\xi(T)$, and the zero-temperature value $\xi(0) \approx 0.18\hbar\nu_f/(k_B T_c)$ [23], where v_f is the Fermi velocity, k_B is the Boltzmann constant, and T_c is the transition temperature. For BCS superconductors, the relationship between T_c and zero-temperature energy gap $\Delta(0)$ is given by $2\Delta(0) = 3.53k_B T_c$ [24]. When temperature is close to T_c, the physics of superconductivity is explained by the Ginzburg-Landau theory [25, 26].

Although there are different superconducting photon detectors for various applications, they are essentially identical in that they break Cooper pairs during detecting photons. In principle, a photon is able to be detected so long as its energy is larger than the binding energy of Cooper pairs $hf > 2\Delta$ [27] (Figure 1), where Δ is the energy gap of superconductors [28]. Generally speaking, the energy resolution of a radiation detector is limited by the statistical fluctuation of the number of electrons or quasiparticles excited by a photon, and it can be approximatively calculated by [29]

$$\Delta E/E = 2.355(\varepsilon F/E)^{0.5}, \tag{1}$$

where F is the Fano factor, and ε is the mean energy required to excite one electron or quasiparticle in the detectors. In (1), ε is positive correlation to the superconducting energy gaps and the semiconducting band gaps. Because the superconducting energy gap (NbN for example) has a magnitude of 3.2 meV [30], which corresponds to millimeter wave, superconducting detectors are able to detect millimeter/submillimeter waves, infrared rays, visible light, X-rays and gamma-rays [31]. Indeed, photons with lower frequencies may also be detected if superconducting materials with lower energy gap are chosen. In comparison, semiconductor band gaps have a magnitude of eV; thus, superconducting detectors

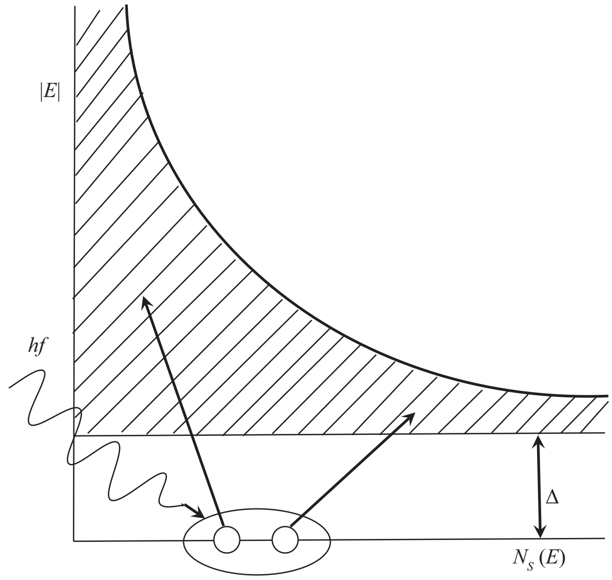

Figure 1 Photons with energy $hf > 2\Delta$ are absorbed by superconducting detectors to break Cooper pairs and create quasiparticles.

Table 1 A comparison of five superconducting detectors

Detectors	Energy resolution	Count rates (cps)	Operating temperature	Decay time	Detection range	References
TES	1.6 eV @ 5.9 keV	$\sim 10^2$	$\sim$ 100 mK	$\sim$ 1 ms	<10 keV	[32, 37–39]
STJs	12 eV @ 5.9 keV	10^3–10^4	0.1 K–1.4 K	$\sim$ 1 µs	<6 keV	[29, 40, 41]
TKIDs	75 eV @ 5.9 keV	$\sim 10^2$	$\sim$ 100 mK	$\sim$ 1 ms	<10 keV	[42, 43]
X-SNSPD	–	$\sim 10^6$	$\sim$ 4 K	$\sim$ 10 ns	<10 keV	[44, 45]
SDDs	$\sim$ 150 eV	$\sim 10^3$	$\sim$ 300 K	$\sim$ 5 µs	<60 keV	[6, 8]

possess a much wider detection waveband than semiconducting detectors with quantum-limit sensitivity, allowing a factor of $\sim$30 improvement in the fundamental resolution.

2 Superconducting detectors for X-ray detection and their applications

X-ray spectroscopy is one of the most sensitive, nondestructive analytical techniques for materials analysis, providing both qualitative and quantitative compositional information [32]. Owing to the fact that the performances of existing semiconducting detectors are gradually becoming unable to satisfy the current needs of some X-ray detection methods, superconducting X-ray detectors are being developed as new generation X-ray spectrometers.

In this section, several superconducting detectors are described in detail, including TES [33], superconducting tunneling junctions (STJs) [34], kinetic inductance detectors (KIDs) [35] and and superconducting nanowire single-photon detectors (SNSPDs) [36]. We primarily analyze their detection mechanisms, compare their physical structures, and introduce related technologies, such as readout electronics. During the discussion, we emphasize TES, which is the most successful superconducting detector for X-ray detection thus far. We also pay special attention to the X-ray absorbers. Additionally, we summarize the recent progress of these four superconducting detectors in X-ray detection. Table 1 [6, 8, 29, 32, 37–45] makes comparison on the response characteristics of above-mentioned X-ray detectors, including their energy resolution, count rates, operating temperature, recovery time, and detection range.

2.1 TES

As an ultrasensitive thermometer, TES makes use of the change of resistance from the superconducting state to the normal state caused by the increase of temperature [39]. Figure 1.3 in [46] is a schematic diagram that illustrates the generation process of the temperature pulse caused by a photon. Without the electro-thermal feedback, the relaxation time for an external signal is nearly equal to the thermal time constant $\tau = \frac{C}{G}$, where C is film heat capacitance and G is conductance. The typical recovery time of TES is the order of ms. When it comes to the energy resolution of TES, it is a little different from (1). Because TES is a calorimeter, and it measures the temperature rise in an isolated heat capacity caused by incident photon. Its fundamental energy resolution can be shown as

$$\Delta E_{\text{FWHM}} = 2.355\sqrt{4\sqrt{\frac{n}{2}}k_B T_e E_{\text{sat}}}, \tag{2}$$

where n is electron-phonon coupling number, $T_e \approx T_c$, and saturation energy $E_{\text{sat}} \approx T_c/\alpha \text{C}$, so its energy resolution is proportional to the square root of the transition temperature.

When TES biases in its transition region, small changes in temperature can cause an obvious increase in resistance, which makes TES a sensitive thermometer over small temperature ranges. The resistance variation that occurs due to temperature can be influenced by many factors, such as external field, the transport current in the film, the magnetic field induced by the transport current, and the fluctuation of temperature caused by Joule heating. When detecting photons, we must reduce their influence on detectors.

TES can be constructed from low- and high-T_c materials, but as shown in (2), high-T_c TES detectors have a lower sensitivity. In this review, we focus on BCS superconductors, the T_c of which are relatively low. The T_c of most TES detectors are below 1 K, and within this temperature range, the film conductance G is explained by the Wiedemann-Franz thermal conductance of normal electrons $G_{WF} = L_0 T/R$, where L_0 is the Lorenz number, T is the temperature, and R is the electrical resistance. The L_0 of superconductor is approximately equal to the normal state value if the temperature is near to T_c, which is determined by the equation [47] $L_0 \approx \pi^2 k_B^2/(3\text{e}^2) = 24.4\ \text{nW}\cdot\Omega\cdot\text{K}^{-2}$. The Joule heating dependence of temperature variation is approximately described by $\delta T \sim P_J/G_{WF}$, where Joule heating power P_J is related to the detector geometry and the structure of the link between detector and heat sink (Figure 2(a)).

The response of TES is governed by electrical and thermal differential equations. The change of temperature T is described by a thermal equation. If the noise terms are ignored, the equation can be written as follows [48]:

$$C\frac{\text{d}T}{\text{d}t} = -P_{\text{bath}} + P_J + P, \tag{3}$$

where C represents the total heat capacity of the TES and the absorber, T is the temperature of the TES sensor, P_{bath} is the power flowing from the TES to the heat bath, P_J is the Joule power dissipation and P is the signal power.

The variation of current I is given by the electrical equation. If the noise terms are ignored, then the equation is as follows:

$$L\frac{\text{d}I}{\text{d}t} = V - IR_L - IR(T, I), \tag{4}$$

where L indicates the inductance, V the Thevenin-equivalent bias voltage [49], I the electrical current through TES, and $R(T, I)$ the electrical resistance of the TES related to both temperature and current, respectively. The solutions of the two equations are discussed in detail by Irwin [50] and Lindeman [49]. As is well-known, it is unconventional to deal with the nonlinear terms in the two differential equations; nevertheless, these nonlinear terms can be approximatively linearized in a small-signal limit in the TES, and the results can be written as follows:

$$R(T, I) \approx R_0 + \alpha_I \frac{R_0}{T_0}\delta T + \beta_I \frac{R_0}{I_0}\delta I, \tag{5}$$

where α_I and β_I are defined independently as the partial derivative parameters. From that, we can conclude that the resistance of TES is connected with temperature and bias current [51].

The geometrical structure of TES detectors includes sensors and absorbers. In summary, sensors are divided into thermal and athermal detectors. TES is a thermal sensor, and the energy fluctuations in a

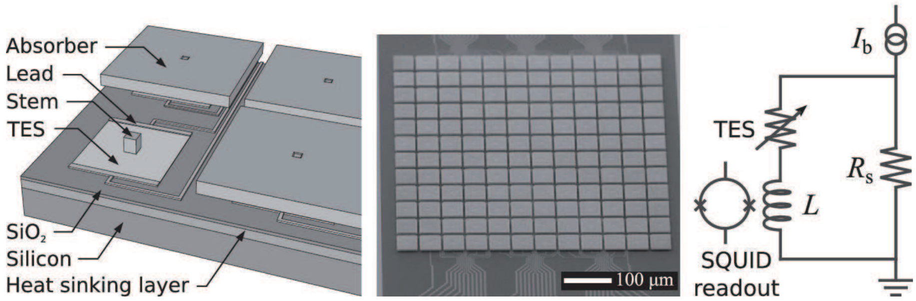

(a) (b) (c)

Figure 2 (a) A schematic diagram of the device showing the detector layers; (b) a scanning electron microscope (SEM) image of the array; (c) read-out circuit diagram [59] @Copyright 2015 AIP Publishing LLC.

thermally isolated heat capacity C at T caused by the exchange of energy with a thermal bath at the same T are given by $(k_BT^2C)^{1/2}$, so the sensitivity of a TES is high when C and T are small [52]. In comparison, both STJs and KIDs are athermal sensors; they measure the generation of quasiparticles caused by the incident photons. However, it is difficult to use STJs in large arrays because they lack a multiplexing readout method. In recent years, KIDs have also been used as thermal sensors (thermal KIDs, TKIDs) [42], which work in a thermal quasi-equilibrium mode [43,53] for X-ray detection, and their photon absorption mechanism is similar to that of TES. The difference is that the microwave multiplexing readout method makes it extremely easy for KIDs to fabricate large arrays. Thus, the resolutions of STJs and KIDs are lower than those of TESs when applied to X-ray detection [54, 55]. We will discuss the related research in detail in Subsections 2.2 and 2.3.

If the photon energy is below 1 keV, it can be absorbed by the superconducting sensor. However, for higher photon energy, an absorber is required. When a photon is absorbed by an absorber, its energy is first transferred to the kinetic energy of an electron, and then, the high-energy electron reduces its energy to the Fermi level through electron-electron and electron-phonon inelastic scattering [56]. Because the energy lost in an electron-phonon inelastic scattering is limited to $\hbar\omega_D$ ∼10 meV by the Debye cutoff frequency ω_D [57], electron-electron inelastic scattering is a more efficient cooling mechanism. The absorbers of superconducting detectors are usually designed on a micro-machined membrane or above the substrates on small-area supports, as shown in Figure 2(a). The absorber on the lower-left pixel is removed for clarity. Figure 2(b) shows a scanning electron microscope (SEM) image of overhanding absorbers for X-ray detection [58, 59]. For superconductors, the high-energy electron relaxation process is often complete within 0.1 ns, so the recovery time is restricted by the process of thermalization. For thermal superconducting detectors, an effective absorber must possess high stopping power, low heat capacity, and good thermalization properties. According to the experimental relation [60]:

$$\mathrm{Re}(E) = \frac{3.52}{\rho}\left(\frac{E}{10\ \mathrm{keV}}\right), \tag{6}$$

where ρ is the density of the material in g/cm^3, and E is the X-ray energy, the photoelectron range $\mathrm{Re}(E)$ of X-ray for a material is related to its atomic number, and heavy atom has a better absorption. Experimentally, gold and semimetal bismuth are widely used as absorbers owing to their high atomic number and low specific heat. As a superconductor, tantalum [61] has a low phononic specific heat and a high atomic number, and is widely used in X-ray absorption. However, the time constant of tantalum is approximately 10^{-2} s or longer [38], which slows the recovery speed of the detectors. In quick-response detection, Sn is a more suitable absorber [62]. In a recent report, multi-absorbers were also used for X-ray astronomy [63].

Because the noise of TES is mismatched with FET amplifiers, TES is rarely used in practical applications. To read out signals with low noise, alternative solutions, such as a cross-correction circuit [64], or long mender lines with high normal resistance, were constructed [65] in the early years. In 2004, Clarke et al. [66] successfully resolved this issue by the use of SQUID current amplifiers, the impedances of which are

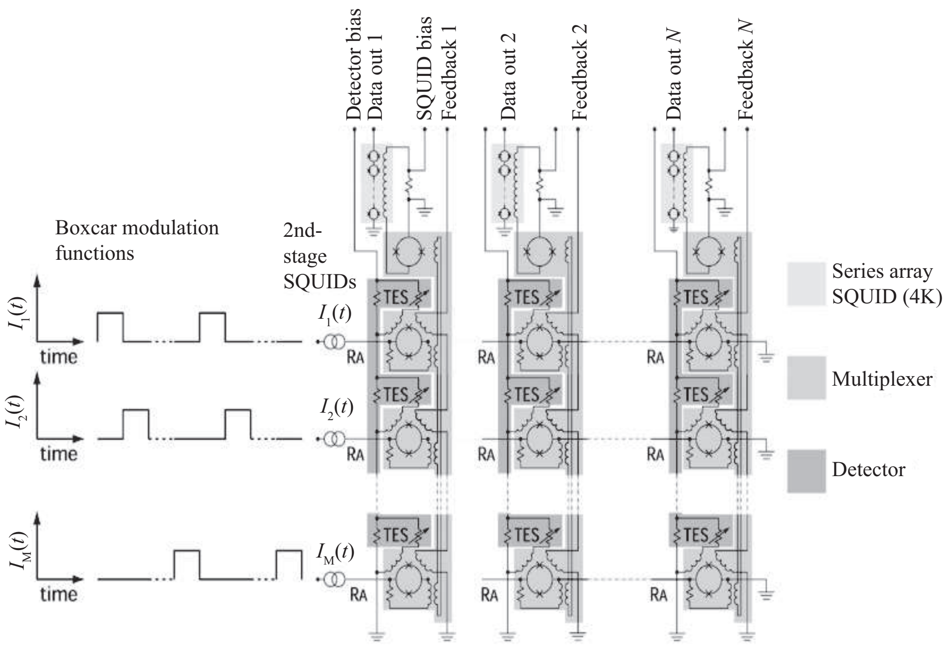

Figure 3 National Institute of Standards and Technology (NIST) time-division multiplexer. Each DC-biased TES detector (dark gray) is coupled to a normally closed SQUID switch (medium gray). The switches on a column are wired in a series to an array SQUID output amplifier (light gray) [74] @Copyright 2003 AIP Publishing LLC.

easily matched with low-resistance TES detectors [67]. Furthermore, SQUIDs make it possible to obtain a multiplex readout of TES arrays, which expands the applications of large TES arrays. In practice, it is not easy for a TES to work within a narrow transition temperature region. Because TES performance is significantly influenced by the bias current and bath temperature fluctuations. However, Irwin has found that if TES is voltage-biased and is read out with a SQUID current amplifier, detector can self-regulate its temperature within the transition and is less sensitivity to bath temperature fluctuations [68].

SQUID amplifiers work at a low temperature, and they are biased and read out with a room temperature electronic circuit. Figure 2(c) shows the typical SQUID readout circuit of one TES. In fact, the output current of the first-stage SQUID is measured by a series-array SQUID. A feedback flux is applied to linearize the first-stage SQUID. Owing to the mutual inductance (usually 50 pH), the first-stage SQUID receives the signal from the TES chip. Moreover, the first-stage SQUID is voltage-biased in series with the input coil of a series-array-SQUID second-stage amplifier, and the series-array SQUID amplifies the signal to the room temperature electronic circuits [20].

In most TES detectors applications, large arrays are needed. For example, some X-ray spectra are limited by the natural width of the underlying emission lines, and to continue developing new technology, increasingly large arrays of TES detectors have been developed. In fact, it is redundant and impractical to read every single TES signal separately, because TES requires a number of wires to connect room-temperature circuits to the low temperature stage, which add heat load and cryogenic complexity. Therefore, multiplexing technologies are required for the readout of TES arrays. Since SQUIDs have begun to be used in the TES readout circuits, four multiplexing methods have emerged: time-division multiplexing (TDM), frequency-division multiplexing (FDM), code-division multiplexing (CDM), and microwave SQUID multiplexing (μMUX).

TDM [69, 70] switches among DC-SQUIDs by applying a bias current to one SQUID at a time. The outputs of all the first-stage SQUIDs are summed into a second-stage SQUID that amplifies the combined signals onto a single output channel, with n current bias lines and m output channels allowing for the measurement of $\mathrm{O}(n \times m)$ detectors. TDM has been the most mature technology to date, and has been widely used for TES array readout [71–73]. Figure 3 [74] shows the typical time-division multiplexer developed by the NIST group [69]. When the boxcar control signal is positive, the corresponding row of switches opens, coupling the outputs of the TESs in the row to their output amplifier. FDM [75, 76] divides multiple input signals into different frequencies on the same output channel and uses cold filter circuits to apply a different oscillating voltage bias to each TES; there are many TES applications [77–79] that use FDM. As a developing multiplexing method, CDM [37, 80] uses an orthogonal basis set intermediately between TDM and FDM. Like TDM, the readout of CDM is divided into multiple timeslots, but the difference is that the signals from all TES chips are collected in each timeslot. μMUX technology [81–84] combines the sensitivity of TESs with the easy multiplexing readout of KIDs, and it makes use of the change in inductance of dissipationless SQUIDs to modulate the resonance frequencies of microwave resonators. Because μMUX allows for larger multiplexing factors compared with the other three multiplexing technologies, in recent years it has become the research object with the most potential and has a lot of possibilities for further development.

Since TES was invented in the 1950s, they have been further developed and have proven to have a wide variety of applications. TES applications can be divided into two categories: bolometric applications and calorimetric applications. TES bolometers mainly perform astronomy in the microwave, sub-mm, terahertz, and far infrared. TES calorimeters have applications on X-ray spectroscopy for materials analysis, imaging X-ray spectroscopy for astronomy, γ-ray spectroscopy for nuclear materials analysis, and α-particle spectroscopy for nuclear forensics [46].

Until the present, the best TES energy resolution for X-ray astronomy was 1.6 eV at 5.9 keV [85]. Figure 4 shows the TES spectrum of the Mn-$K\alpha$ X-ray lines complex near 5900 eV [86]. An improvement to $\Delta E_{\rm FWHM} < 3$ eV is readily achievable with minor modification to the experimental setup [87, 88]. By this study, three variations are constructed and indicate that it is possible to manipulate the transition width and G independently, thus enabling fast thermal sensors with excellent energy resolution.

Another application of TES detectors is X-ray spectroscopy for materials analysis. Figure 5 shows the diagram of TES microcalorimeter [32]. For clarity, translation stages and microcalorimeter heat shields are not shown. Figure 6 shows the TES microcalorimeter EDS (μcal EDS, solid line) result of WSi_2 mounted on a SEM and the semiconductor EDS spectrum (dashed line) result of WSi_2. The TES microcalorimeter EDS spectrum is acquired using a thin ($\approx$100 nm) WSi_2 film on SiO_2 as part of the multiple element data set, and has been corrected for energy nonlinearity. The energy bandwidth per channel varies from 2.1 to 2.4 eV over the energy range 1300–2300 eV. The impressive increase in resolution over that of semiconductor EDS, coupled with reasonable output count rates and a solid angle, demonstrates the usefulness of TES microcalorimeter EDS for X-ray microanalysis [32, 89].

2.2 STJs

Cross-film-type Sn/SnO_x/Sn STJs were first used by Wood and White in 1969 to detect α particles detection [90]. Since then, STJs have been extensively studied as photon detectors in the X-ray region of the spectrum [91]. Structurally, STJs consist of two superconducting films separated by a thin insulating barrier, as shown in Figure 7. The usual layers are as follows: Nb/Al/I/Al/Nb, and I is a tunnel barrier (Al_2O_3). In some times, Nb is replaced by Ti [92]. Even more complex sequences of layers, such as Ti/Nb/Al/I/Al/Nb/NbN, have since been proposed. The multilayer superconducting films on both sides of the barrier can effectively prevent the generated quasiparticles from escaping through the electrodes. The thickness of one electrode is 100$\sim$300 nm, which ensures the high probability of nonequilibrium quasiparticles tunneling. However, a small thickness limits the use of STJs to the range of soft X-rays and the ultra violet range [40].

The basic features of STJs are well described by the dynamic Cooper-pair breaking and the relaxation mechanisms of nonequilibrium superconductivity [93]. The processes are shown in Figures 8(a) and (b). X-ray absorbed in either of the films of a superconducting junction yield pulses with an identical sign. If an X-ray is absorbed in the film at the higher potential side, the process in Figure 8(a) is responsible for the signal. In the other case, the electrons will tunnel as shown in Figure 8(b). Furthermore, excess quasiparticles are exchanged back and forth, with the quasiparticles always tunneling in the same direction. If the tunneling rate is faster than the effective quasiparticle lifetime, the back and forth

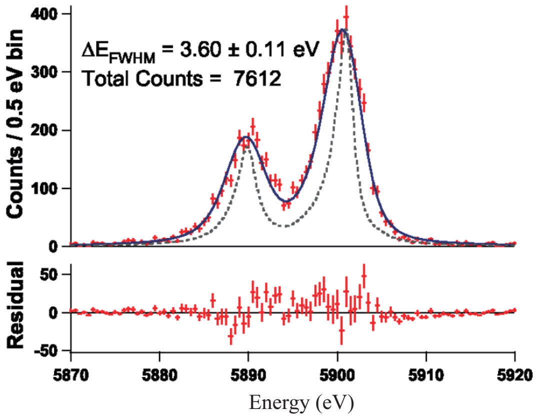

Figure 4 (Color online) Spectrum of MnKα X-rays from an ^{55}Fe source collected using a 490 µm-wide pixel operated at $T_b = 54$ mK and $R = 12.5\%$ R_n. This device has 75% membrane perforation with $G_b = 175$ pW/K. The solid line shows a fit to the data and the dashed line shows the MnKα natural line shape [86] @Copyright 2009, AIP Publishing LLC.

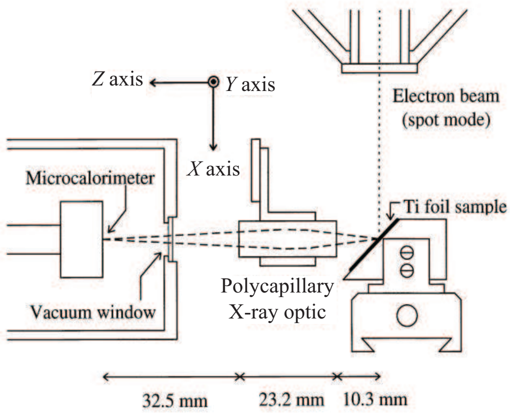

Figure 5 Diagram (approximately to scale) of TES microcalorimeter, polycapillary X-ray optic and Ti foil sample inside the SEM chamber. The polycapillary optic has an input capture angle of 13.48°, an input focal spot width of <100 mm (FWHM), an output convergent angle of 5.78°, and an output focal spot width of <380 mm (FWHM) [32] @Copyright 1997 John Wiley & Sons, Inc.

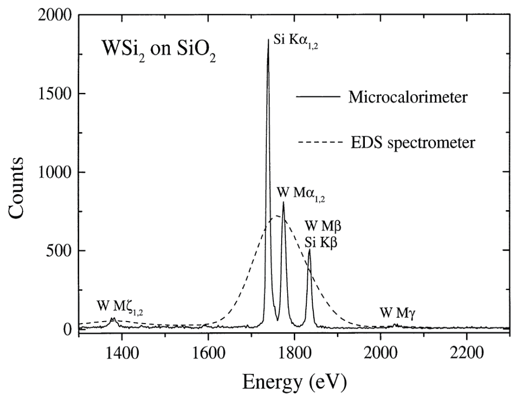

Figure 6 TES microcalorimeter EDS (solid line) of WSi_2, acquired under the following conditions: 10 keV beam voltage, 25.6 nA beam current, input count rate of 180 ± 20 s^{-1}, output count rate of 130 ± 10 s^{-1}, dead time of $28 \pm 5\%$, live time 200 s, specimen-detector distance of 37 ± 2 mm, and a total of 34511 counts. Also shown for comparison is a semiconductor EDS spectrum of WSi_2 [32] @Copyright 1997 John Wiley & Sons, Inc.

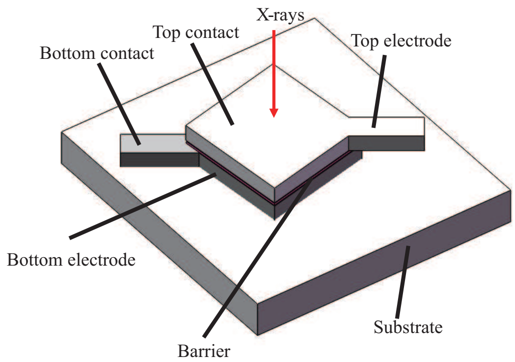

Figure 7 (Color online) The scheme of STJs detector.

processes will result in an intrinsic amplification of the tunneling current [94]. The tunneling will stop when the quasiparticles recombine into Cooper pairs, and the 2Δ phonons released by the recombination escape from films to substrates.

The detection mechanism of STJs is such that when the external superconducting layer absorbs incident photons, the Cooper pairs in said layer will be broken into quasiparticles, and as the quasiparticles flow through the barrier, there will be a current pulse, as shown in Figure 9 [90]. The current pulse height is proportional to the number of quasiparticles N, which is related to the energy of incident photon E, and can be calculated by the following equation [95]:

$$N = \frac{E}{1.73\varepsilon}, \tag{7}$$

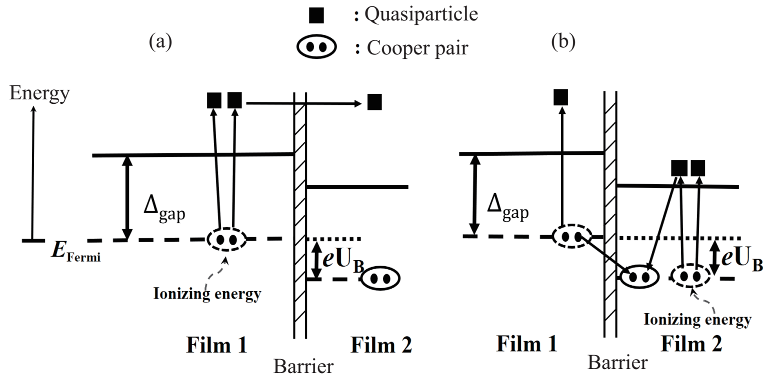

Figure 8 Tunneling processes in a junction with both films superconducting. In both cases, the electrons flow in the same direction. This leads to the observation that X-rays absorbed in either of the films yield a signal with identical sign [93] @Copyright 1986 American Physical Society.

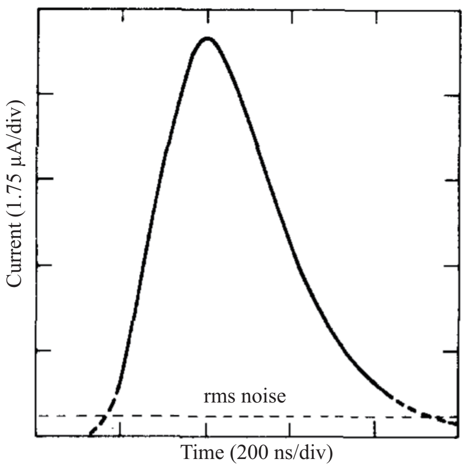

Figure 9 Tracing from a photograph of the output pulse induced by an α-particle traversing junction. Dotted line represents the rms (root-mean-square) noise output from the amplifiers. Vertical scale calibrated by driving known step function currents through lumped constant small signal equivalent of the junction [90] @Copyright 1969 AIP Publishing LLC.

where ε is the binding energy of the Cooper pairs. In this case, an external magnetic field ($\sim$100 Oe, parallel to the barrier layer) should be applied to suppress the Cooper pairs' tunneling current.

Typically, the working temperature of STJs is 0.1$\sim$1.4 K, and the active detection area is about 0.01 mm^2. The main applications of STJs are in low-energy regions, which are less than 6 keV, especially when detecting soft X-ray of light elements from Beryllium to Fluorine, where the energy resolution of 10$\sim$20 eV makes it easy to distinguish between the contributions of various elements. In practice, STJ X-ray detectors can achieve high energy resolution (12 eV at 5.9 keV, shown in Figure 10 [96]) and high time resolution ($<$ 1 μs) [97]. However, the detection area of each STJ chip is small, and the lack of a multiplexing readout method restricts the application of STJs to large arrays.

2.3 KIDs

KIDs were first proposed by Day in 2003. Initially, KIDs were widely used to detect cosmic microwave background (CMB) because they have large area arrays integration compared with other superconducting detectors. Over the past decade, it has been found that the detection waveband of KIDs is very wide, ranging from low-energy THz to high-energy X-ray [31], which is determined by the superconducting energy gap.

Because the operating temperature of KIDs is below $T_c/5$ (approximately several hundred mK), the result is a relatively long quasiparticle lifetime and recovery time ($\sim$100 μs for Al KIDs) [98]. The core

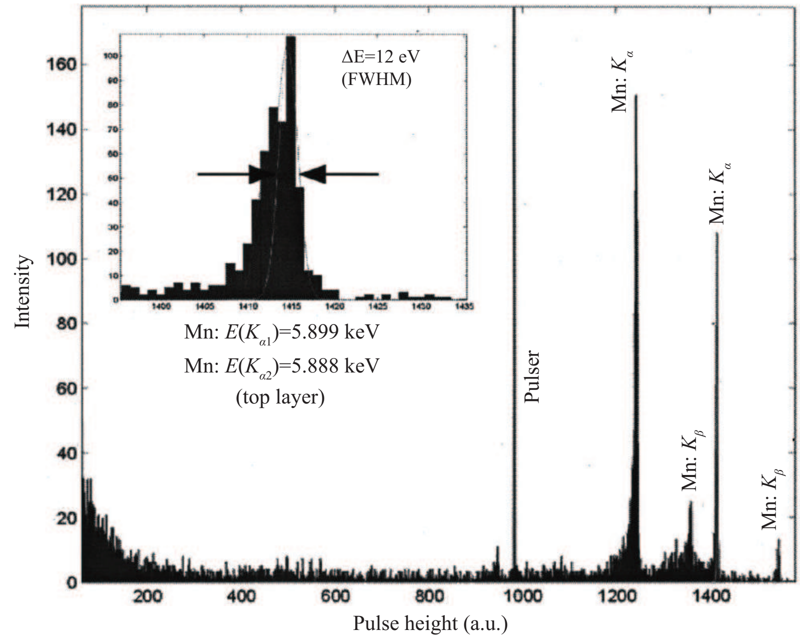

Figure 10 Pulse height spectrum from a single aluminium STJs illuminated by the ^{55}Mn X-ray lines complex. The inset shows a close-up view of the $K_{\alpha 1}$ and $K_{\alpha 2}$ lines from channel 1400 to 1430 of the top layer. The energy resolution for the $K_{\alpha 1}$ line was fitted with ΔE= 12 eV (FWHM) [96] @Copyright 2001 AIP Publishing LLC.

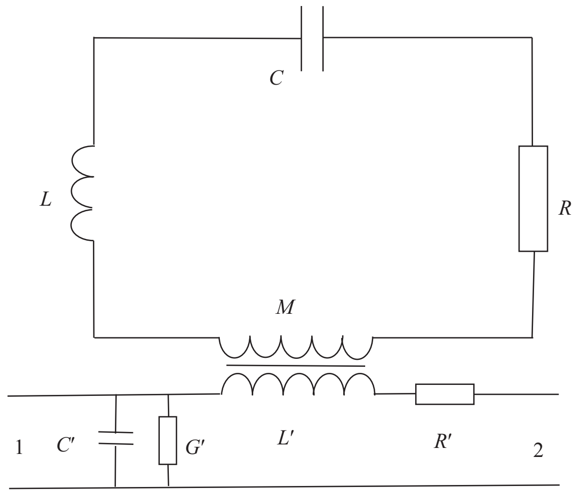

Figure 11 Equivalent circuit diagram of a KID.

unit of KIDs is a superconducting LC resonance circuit, and the equivalent circuit diagram is shown in Figure 11. When working on resonance and in a thermal equilibrium condition, the KID couples to the two-port transmission line by mutual inductance or capacity, producing a dip in its transmission parameter S_{21} [99]. Once receiving photons with energy higher than 2Δ, the Cooper pairs in KIDs will be broken into quasiparticles. The appearance of quasiparticles results in the increase of kinetic inductance L_k in KIDs, and this leads to a shift in the frequency of the resonator [100] as follows:

$$\Delta f_0 = -\frac{1}{2}\frac{1}{L_k + L_g} f_0 \Delta L_k, \tag{8}$$

where $f_0 = \frac{1}{\sqrt{(L_g+L_k)c}}$ is the resonance frequency of KIDs; L_g is geometrical inductance, which is not connected to the temperature; and ΔL_k is a change in quasiparticle density, which can be calculated by the change in the complex part of conductivity (σ_2) [101]. Because the quality factor of superconducting resonators is very high ($\sim 10^4$), the resonance peaks of KIDs are extremely sharp, which means KIDs

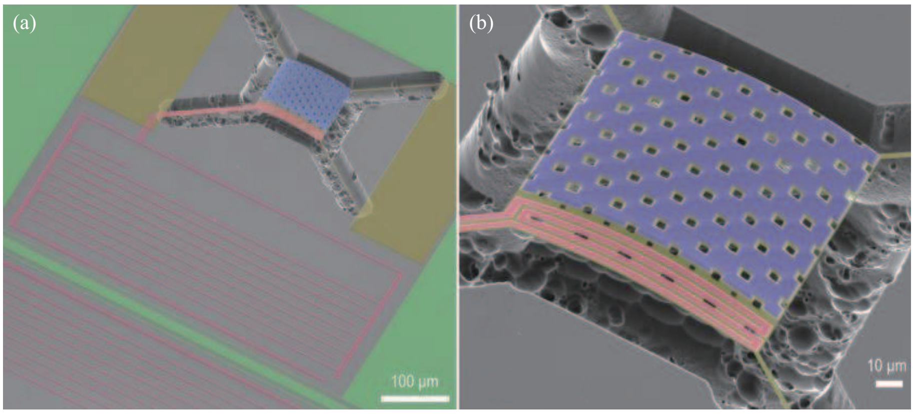

Figure 12 (Color online) (a) A TKID on a silicon substrate; (b) SEM of a TKID island [42] @Copyright 2015 AIP Publishing LLC.

can respond to a slight shift of resonance frequency. This, in turn, means that KIDs are sensitive to small signal. By making the superconductor part of a resonance circuit, it is possible to read out changes in the complex surface impedance of the superconductor owing to radiation absorption as a change in microwave transmission. We can read hundreds or thousands of KID resonators using one microwave transmission line; thus, the readout circuit of KID arrays is very concise.

In the primeval design, the resonance circuit of KIDs consists of two parts: a quarter wavelength resonator and an antenna area to absorb photons [102]. However, this structure requires an additional antenna absorbing area to couple the signal to resonators; nevertheless, the quarter wavelength resonator is usually geometrically small, so sufficient quasiparticles are not produced by photons absorption. In most cases, two different superconducting materials are needed in these KIDs. During the response processing, the quasiparticles produced by the higher energy gap superconductor, such as Nb, can excite more quasiparticles in the lower energy gap superconductor, such as Al, which can result in a larger increase in L_k. These two aspects complicate the preparation of films and devices.

In 2008, Simon Doyle designed the lumped element kinetic inductance detector [103] (LEKIDs), which is a device that directly absorbs photons and can serve as an alternative to distributed antenna coupled quarter wavelength resonators. Additionally, it is easy for LEKIDs to couple several hundred absorbing micro-resonators on a single transmission line; thus, they can be read out by frequency division multiplexing [35], which enables the design of large pixel arrays. A single pixel LEKID is composed of a long meander line and an interdigital capacitor [104]. Because a LEKID chip is a two-dimensional structure, and its minimum geometric size is a magnitude of μm, it is easy to fabricate large LEKID arrays.

To apply KIDs in X-ray detection, an extra absorber is required. In 2015, a research group from UCSB [42] reported TKIDs to detect X-ray, the physical structure of which is shown in Figure 12. Interdigitated capacitors and meandered inductors are etched from 200 nm of sub-stoichiometric TiN_x. These form LC circuits, each with a unique resonance frequency, coupled to a CPW Nb (green) feed line. The inductors, and separate 500 nm thick Ta (blue) absorbers sit on a free-standing Si_3N_4 (yellow) island. The Ta absorber and the Si_3N_4 beneath it are perforated to facilitate under-etching with XeF_2. They etch 10$\sim$15 μm into the Si. The thin Si_3N_4 bridges holding the free-standing island have a cross section of 2.0 μm$\times$0.25 μm and are 141 μm long. In this study, they presented a TKID prototype that uses Tantalum as an X-ray absorber and achieved an energy resolution of 75 eV at 5.9 keV (Figure 13). TKIDs have been recently developed as superconducting X-ray detectors [43, 53], and they have the potential to achieve excellent energy resolution and can be scaled up to kilo- or even mega-pixel arrays [105]. The only issue is that TKIDs suffer a low-energy resolution and a low count rate, which scientists are attempting to solve using cantilevered three-dimensional (3D) absorbers [106], and suppressing two-level system noise [107–109] with a large capacitor. Because many modern applications of X-ray imaging spectroscopy require both high energy and spatial resolution over a large field of view, TKIDs can bring enormous improvements to these fields as rapidly developing detectors.

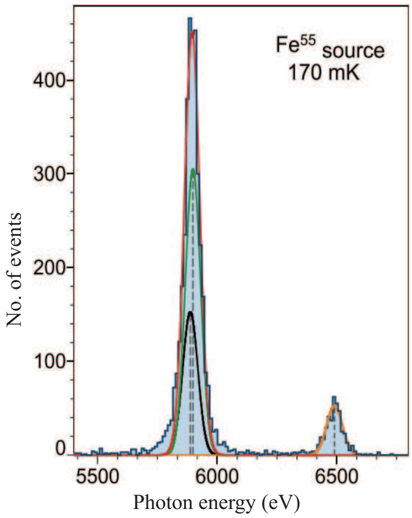

Figure 13 (Color online) Distribution of the fitted energies of 4970 absorbed X-ray photons from a Fe^{55} source, measured at 170 mK. Based on the line splitting and the average line width, we calculate an energy resolution of 75 eV at 5.9 keV [42] @Copyright 2015 AIP Publishing LLC.

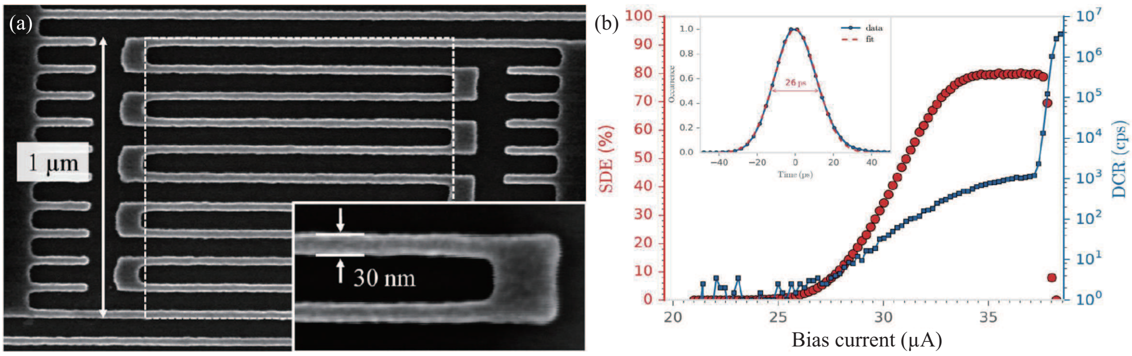

Figure 14 (Color online) (a) SEM images of an SNSPD hydrogen silsesquioxane mask on NbN. The nanowires are 30 nm wide, and the pitch is 100 nm (inset), covering an active area of 1.03 μm×1.14 μm (dashed frame) [110] @Copyright 2011 American Chemical Society. (b) System detection efficiency (red circles) and the dark count rate (blue squares) as a function of the bias current [111] @Copyright 2018 AIP Publishing LLC.

2.4 SNSPD

In 2001, Goltsman developed an SNSPD to detect single photon, and it has potential applications in spectroscopy, optical fiber sensing, and quantum communication. The geometrical structure of an SNSPD is shown in Figure 14(a) [110]. The main part of the SNSPD is the meander nanowire. Compared with other single photon detectors, SNSPD possesses higher detection efficiency and a lower dark count rate (Figure 14(b)). In addition, the recovery time and jitter time of SNSPD are faster than those of existing single-photon detectors [111].

Although the operating temperature of SNSPD is below $T_c/2$, the T_c of SNSPD is high, which makes it possible for SNSPD to work at the boiling point of liquid helium, which is an obvious advantage over other superconducting detectors. The detection mechanism of SNSPD can be described as follows [36,112,113]. The nanowire is maintained below $T_c/2$ and persistently biased by a transport current just below the I_c ((i) in Figure 15(a) [114]). When a photon with an energy higher than 2Δ irradiates on the nanowire, Cooper pairs will be broken into quasiparticles, and the generated quasiparticles form a hotspot ((ii) in Figure 15(a)). As a result, the hotspot region forces the supercurrent to flow around the resistive region ((iii) in Figure 15(a)), which leads to an increase of the current density beyond the critical current density in the sidewalks; this results in a resistive barrier across the width of the nanowire ((iv) in Figure 15(a)). In Figure 15(b), L_k is the kinetic inductance of the superconducting nanowire and R_n is

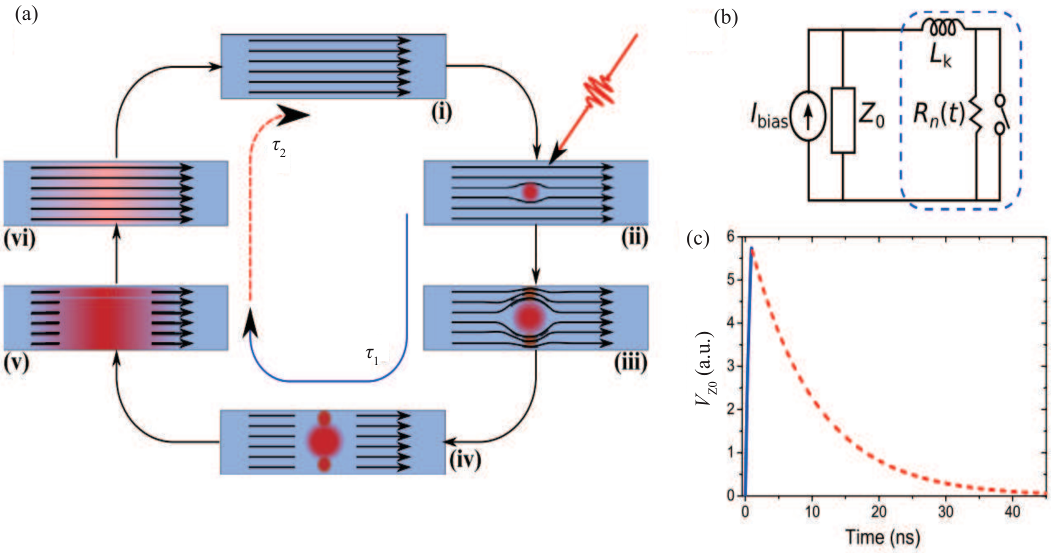

Figure 15 (Color online) The basic operation principle of the SNSPD. (a) A schematic illustrating the detection cycle; (b) a simple electrical equivalent circuit of a SNSPD; and (c) a simulation of the output voltage pulse of the SNSPD [114] @Copyright 2012 IOP Publishing Ltd.

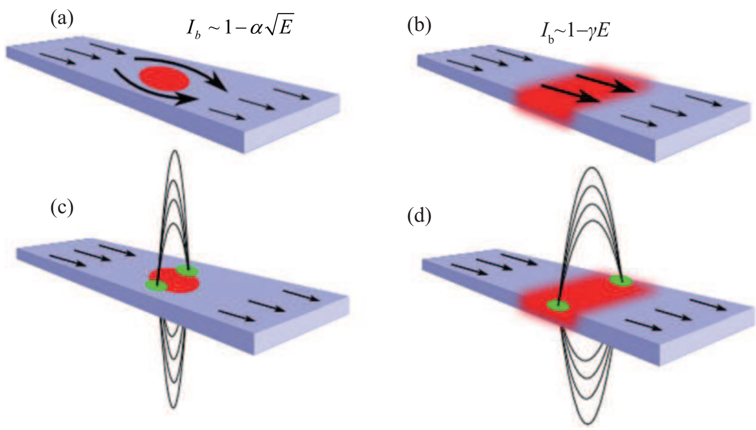

Figure 16 (Color online) Sketches of the four main detection models. (a) The normal-core hot spot model; (b) the diffusion-based hot spot model; (c) the vortex nucleation model; and (d) the vortex crossing model [115] @Copyright 2014 American Physical Society.

the hotspot resistance of the SNSPD. The SNSPD is current biased at I_{bias}. Opening and closing the switch simulates the absorption of a photon. An output pulse is measured across the load resistor Z_0. The sudden increase in resistance from zero to a finite value generates a measurable voltage pulse across the nanowire (Figure 15(c)). Subsequently, the energy dissipates into the substrate by the phonon in the superconductor owing to continuous cooling, and SNSPD recovers to superconducting state [36, 112, 113].

As shown in Figure 16, four models exist to explain the mechanisms of SNSPD [115]. (a) Normal core hot-spot model: The incident photon causes a cylindrical volume inside the wire to transition to the normal state [116]. (b) Diffusion-based hot-spot model: The quasiparticles diffuse outward from the point of absorption, creating a band of depleted superconductivity [117]. (c) Vortex-nucleation model: A vortex-antivortex pair is formed in the hot spot, which can result in the generation of resistance [118]. (d) Vortex crossing model: Either a vortex or a vortex-antivortex pair uses an area of weakened superconductivity to cross the wire, after which there will be a resistance [119].

Regarding the applications of SNSPD, it is a promising alternative for time-correlated single-photon counting at infrared wavelengths, offering single-photon sensitivity combined with low DCR, low timing

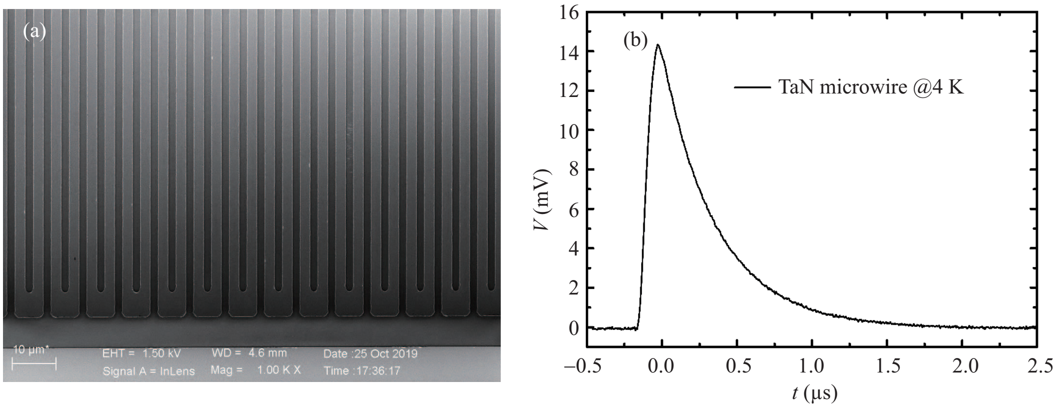

Figure 17 (a) SEM image of a partial 100-nm TaN SSPD. The microwires are 2.2 μm wide, and the pitch is 1.8 μm, covering an active area of 2.25 mm×2.25 mm. (b) A response pulse of this TaN SSPD for a Fe^{55} X-ray source.

jitter Δt (tens of ps), short recovery time, and free-running operation [120]. In recent years, SNSPD has also been used to detect X-rays; in such situations, it is referred to as X-SNSPD [45], the geometrical structure of which is similar to that of a normal SNSPD. The latest result of X-SNSPD was shown in [44, 121]. In this study, WSi based SNSPD possesses a high maximum counts-per-second-per-square-millimeters of 10^6 cps and can work at a T_c just below 5 K, even above the boiling temperature of liquid helium.

Because X-SNSPD possesses high count-rate, short recovery time, and high operating temperature, it has a promising prospect in X-ray sensitive detection and attracts our attention. We designed a superconducting strip-line detector (SSLD), whose structure is similar to SNSPD. Experimentally, TaN was used to fabricate SSLD to improve the absorption efficiency. In comparison, our TaN SSLD is wider, longer, and thicker than X-SNSPD.

While studying the TaN X-SSLD, we obtained encouraging results. The SEM image of TaN microwires is shown in Figure 17(a). The thickness of this detector is 100 nm, and the total length of the TaN microwire is 1.57 m. Figure 17(b) shows the response pulse at 4 K of our TaN SSLD for a Fe^{55} X-ray source. The response was approximately 500 ns, which means this detector has higher count rates than other existing superconducting X-ray detectors, and this detector can also work around the boiling point of liquid helium (4.2 K), which significantly reduces the refrigeration costs. Moreover, owing to large active areas, the kinetic inductance of this detector is large, which solves the latching problems of X-SNSPD at a high bias current and facilitates the reading out of the output signal. In fact, this detector does not latch at 90% I_c. Furthermore, the dark count rates of this detector are as low as 2×10^{-4} s^{-1}; thus, it appears that SNSPD has significant potential to be used in X-ray detection. At present, X-SNSPD suffers a low detection efficiency of $\approx$ 7.5% owing to the lack of an X-ray absorber and latching at high bias current. In addition, the fact that the X-SNSPD has no energy resolution is an urgent problem. Therefore, there is still a lot of room for X-SNSPD development.

3 Summary and outlook

We have presented a review of superconducting X-ray detectors, including TES, STJs, KIDs, and SNSPD. Specifically, we have focused on the device physics, geometrical structures, readout electronics, and X-ray detection applications of these four detectors. TES detectors have the highest energy resolution along with a relatively long recovery time. STJs show good comprehensive performances in soft X-ray spectroscopy and count rates. As potential detectors, KIDs reveal superiority in the multiplexing readout of large arrays, while SNSPD is advantageous in terms of count rates and cooling costs.

The past two decades have seen momentous progress in the use of superconducting detectors in X-ray detection owing to the development of refrigeration technology. However, there is still room to improve the understanding of the physics and detection performance of said detectors. Thus far, there are no superconducting X-ray detectors that can achieve good performances regarding both energy resolution and count rates, which are urgently needed in elemental analysis and synchrotron science. In general, further improvements in spectrometer count rates and readouts of large arrays are necessary for existing superconducting X-ray detectors. Based on these requirements, scientists have recently attempted to improve how well these superconducting detectors perform when it comes to X-ray detection by combining their respective characteristics. TES and X-SNSPD can make up their lacks in readouts of large arrays by using KIDs' microwave multiplexing readout circuit. X-SNSPD can add relevant absorbers to improve its absorbing efficiency for X-ray. TKIDs may achieve better detection sensitivity by using larger capacitor and cantilevered absorbers with high fill factor. Besides, it is possible to reduce the recovery time of detectors and improve their count rates by using popular perovskite nanocrystal scintillators to replace the existing absorbers, which can change the X-ray absorbing method from photo-thermal conversion to light-light conversion. As science and technology continue to develop, there is no question that superconducting detectors will significantly improve and play an increasingly important role in X-ray detection applications in the near future.

Acknowledgements This work was supported by National Key R&D Program of China (Grant No. 2017YFA0304000), National Natural Science Foundation of China (Grant Nos. 61671438, U1631240), Shanghai Municipal Science and Technology Major Project (Grant No. 2019SHZDZX01), and Program of Shanghai Academic/Technology Research Leader (Grant No. 18XD1404600).

References

1 Hasegawa B H. The Physics of Medical X-ray Imaging, Or, the Photon and Me–How I Saw the Light. 2nd ed. Madison: Medical Physics, 1991

2 Jenkins R, Snyder R L. Introduction to X-ray Powder Diffractometry. New York: Wiley, 1996

3 Wang Q, Chen Z, Wu X, et al. Review of X-ray security inspection technology. Compu Tomograph Theory Appl, 2004, 1: 8

4 Fraser G. X-ray Detectors in Astronomy. Cambridge and New York: Cambridge University Press, 1989. 312

5 Cnudde V, Boone M N. High-resolution X-ray computed tomography in geosciences: a review of the current technology and applications. Earth-Sci Rev, 2013, 123: 1–17

6 Jenkins R. X-ray Fluorescence Spectrometry. New York: Wiley, 1999

7 Gatti E, Rehak P. Semiconductor drift chamber — an application of a novel charge transport scheme. Nucl Instruments Methods Phys Res, 1984, 225: 608–614

8 Lechner P, Fiorini C, Hartmann R, et al. Silicon drift detectors for high count rate X-ray spectroscopy at room temperature. Nucl Instruments Methods Phys Res Sect A-Accelerators Spectrometers Detectors Associated Equipment, 2001, 458: 281–287

9 Lechner P, Eckbauer S, Hartmann R, et al. Silicon drift detectors for high resolution room temperature X-ray spectroscopy. Nucl Instruments Methods Phys Res Sect A-Accelerators Spectrometers Detectors Associated Equipment, 1996, 377: 346–351

10 Yakunin S, Sytnyk M, Kriegner D, et al. Detection of X-ray photons by solution-processed lead halide perovskites. Nat Photon, 2015, 9: 444–449

11 Tinkham M. Introduction to Superconductivity. 2nd ed. New York: McGraw-Hill, 1996

12 Schrieffer J R. Theory of Superconductivity. Boca Raton: CRC Press, 2018

13 Matthias B T, Geballe T H, Compton V B. Superconductivity. Rev Modern Phys, 1963, 35: 1

14 Anlage S M. The physics and applications of superconducting metamaterials. J Opt, 2010, 13: 024001

15 Tomita M, Murakami M. High-temperature superconductor bulk magnets that can trap magnetic fields of over 17 tesla at 29K. Nature, 2003, 421: 517–520

16 Braunisch W, Knauf N, Kataev V, et al. Paramagnetic Meissner effect in Bi high-temperature superconductors. Phys Rev Lett, 1992, 68: 1908

17 Orlando T P, Delin K A. Foundations of Applied Superconductivity. Reading: Addison-Wesley, 1991

18 Semenov A, Engel A, Ilin K, et al. Ultimate performance of a superconducting quantum detector. Eur Phys J Appl Phy, 2003, 21: 171–178

19 Bardeen J, Cooper L N, Schrieffer J R. Theory of superconductivity. Phys Rev, 1957, 108: 1175–1204

20 Irwin K D, Hilton G C. Transition-edge sensors. In: Cryogenic Particle Detection. Berlin: Springer, 2005. 63–150

21 Aschermann G, Friederich E, Justi E, et al. Supraleitfähige Verbindungen mit extrem hohen Sprungtemperaturen (NbH und NbN). In: Technischwissenschaftliche Abhandlungen der Osram-Gesellschaft. Berlin: Springer, 1943. 401–416

22 Andrews D, Brucksch J W, Ziegler W, et al. Superconducting films as radiometric receivers. Phys Rev, 1941, 59: 1045
23 Pippard A. Field variation of the superconducting penetration depth. Proc Royal Society London Ser A Math Phys Sci, 1950, 203: 210–223
24 Suhl H, Matthias B T, Walker L R. Bardeen-Cooper-Schrieffer theory of superconductivity in the case of overlapping bands. Phys Rev Lett, 1959, 3: 552–554
25 Gor'kov L P. Microscopic derivation of the Ginzburg-Landau equations in the theory of superconductivity. Sov Phys JETP, 1959, 9: 1364–1367
26 Ginzburg V, Landau L. Zh. Eksper. Teor. Fiz. Oxford: Pergamon Press, 1950, 20: 1064–1082
27 Day P K, LeDuc H G, Mazin B A, et al. A broadband superconducting detector suitable for use in large arrays. Nature, 2003, 425: 817–821
28 Zmuidzinas J. Superconducting microresonators: physics and applications. Annu Rev Condens Matter Phys, 2012, 3: 169–214
29 Samedov V V. Influence of the proximity effect on the energy resolution of STJs. Nucl Instruments Methods Phys Res Sect A-Accelerators Spectrometers Detectors Associated Equipment, 2004, 520: 257–259
30 Wang Z, Kawakami A, Uzawa Y. NbN/AlN/NbN tunnel junctions with high current density up to 54 kA/cm^2. Appl Phys Lett, 1997, 70: 114–116
31 Mazin B A, Bumble B, Meeker S R, et al. A superconducting focal plane array for ultraviolet, optical, and near-infrared astrophysics. Opt Express, 2012, 20: 1503–1511
32 Wollman D A, Irwin K D, Hilton G C, et al. High-resolution, energy-dispersive microcalorimeter spectrometer for X-ray microanalysis. J Microsc, 1997, 188: 196–223
33 Irwin K D, Hilton G C, Wollman D A, et al. X-ray detection using a superconducting transition-edge sensor microcalorimeter with electrothermal feedback. Applied Phys Lett, 1996, 69: 1945–1947
34 Kurakado M. Review on superconducting tunnel junctions as ionizing-radiation detectors. In: Superconducting Devices and Their Applications. Berlin: Springer, 1992. 466–473
35 Mazin B A. Microwave kinetic inductance detectors. Dissertation for Ph.D. Degree. California: California Institute of Technology, 2005
36 Gol'tsman G N, Okunev O, Chulkova G, et al. Picosecond superconducting single-photon optical detector. Appl Phys Lett, 2001, 79: 705–707
37 Irwin K D, Niemack M D, Beyer J, et al. Code-division multiplexing of superconducting transition-edge sensor arrays. Supercond Sci Technol, 2010, 23: 034004
38 Irimatsugawa T, Hatakeyama S, Ohno M, et al. High energy gamma-ray spectroscopy using transition-edge sensor with a superconducting bulk tantalum absorber. IEEE Trans Appl Superconduct, 2014, 25: 1–3
39 Ullom J N, Bennett D A. Review of superconducting transition-edge sensors for x-ray and gamma-ray spectroscopy. Supercond Sci Technol, 2015, 28: 084003
40 Friedrich S, Harris J, Warburton W K, et al. 112-pixel arrays of high-efficiency STJ X-ray detectors. J Low Temp Phys, 2014, 176: 553–559
41 Andrianov V. Comment on "Observation of nuclear gamma resonance with superconducting tunnel junction detectors"[AIP Advances 6, 025315 (2016)]. AIP Adv, 2019, 9: 059101
42 Ulbricht G, Mazin B A, Szypryt P, et al. Highly multiplexible thermal kinetic inductance detectors for x-ray imaging spectroscopy. Appl Phys Lett, 2015, 106: 251103
43 Faverzani M, Cruciani A, D'Addabbo A, et al. Thermal kinetic inductance detectors for soft X-ray spectroscopy. Nucl Instruments Methods Phys Res Sect A-Accelerators Spectrometers Detectors Associated Equipment, 2019, 936: 197–198
44 Zhang X, Wang Q, Schilling A. Superconducting single X-ray photon detector based on $W_{0.8}Si_{0.2}$. AIP Adv, 2016, 6: 115104
45 Inderbitzin K, Engel A, Schilling A, et al. An ultra-fast superconducting Nb nanowire single-photon detector for soft X-rays. Appl Phys Lett, 2012, 101: 162601
46 Mates J A B. The microwave SQUID multiplexer. Dissertation for Ph.D. Degree. Colorado: University of Colorado, 2011
47 Chester G V, Thellung A. The law of Wiedemann and Franz. Proc Phys Soc, 1961, 77: 1005–1013
48 Lindeman M A, Bandler S, Brekosky R P, et al. Impedance measurements and modeling of a transition-edge-sensor calorimeter. Rev Sci Instruments, 2004, 75: 1283–1289
49 Lindeman M A. Microcalorimetry and the transition-edge sensor. Dissertation for Ph.D. Degree. Livermore: Lawrence Livermore National Lab., 2000
50 Irwin K D. Phonon-mediated particle detection using superconducting tungsten transition-edge sensors. Dissertation for Ph.D. Degree. Batavia: Fermi National Accelerator Lab., 1995
51 Irwin K D, Hilton G C, Wollman D A, et al. Thermal-response time of superconducting transition-edge microcalorime-

ters. J Appl Phys, 1998, 83: 3978–3985
52 Mandl F. Statistical Physics. 2nd ed. Trowbridge: John Wiley & Sons, 1988
53 Giachero A, Cruciani A, D'Addabbo A, et al. Development of thermal kinetic inductance detectors suitable for X-ray spectroscopy. J Low Temp Phys, 2018, 193: 163–169
54 Mazin B A, Bumble B, Day P K, et al. Position sensitive X-ray spectrophotometer using microwave kinetic inductance detectors. Appl Phys Lett, 2006, 89: 222507
55 Verhoeve P, Martin D, Venn R. Imaging soft X-ray spectrometers based on superconducting tunnel junctions. In: Proceedings of SPIE, 2010. 7742
56 Semenov A D, Gol tsman G N, Sobolewski R. Hot-electron effect in superconductors and its applications for radiation sensors. Supercond Sci Technol, 2002, 15: R1–R16
57 Koch H, Lübbig H. Superconducting devices and their applications: In: Proceedings of the 4th International Conference SQUID'91 (Sessions on Superconducting Devices), Berlin, 1991
58 Hays-Wehle J P, Lowell P J, Schmidt D R, et al. An overhanging absorber for TES X-ray focal planes. IEEE Trans Appl Superconduct, 2017, 27: 1–4
59 Lee S J, Adams J S, Bandler S R, et al. Fine pitch transition-edge sensor X-ray microcalorimeters with sub-eV energy resolution at 1.5 keV. Appl Phys Lett, 2015, 107: 223503
60 Gaidis M. Superconducting tunnel junctions as single photon X-ray detectors. Dissertation for Ph.D. Degree. New Haven: Yale University, 1994
61 Sellers G J, Anderson A C, Birnbaum H K. Anomalous heat capacities of niobium and tantalum below 1 K. Phys Rev B, 1974, 10: 2771–2776
62 O'Neal H R, Phillips N E. Low-temperature heat capacities of indium and tin. Phys Rev, 1965, 137: A748–A759
63 Smith S J, Adams J S, Bandler S R, et al. Multiabsorber transition-edge sensors for x-ray astronomy. J Astron Telesc Instrum Syst, 2019, 5: 021008
64 Maul M K, Strandberg M W P, Kyhl R L. Excess noise in superconducting bolometers. Phys Rev, 1969, 182: 522–525
65 Neuhauser B, Cabrera B, Martoff C J, et al. Phonon-mediated detection of Alpha particles with aluminum transition edge sensors. Jpn J Appl Phys, 1987, 26: 1671
66 Clarke J, Braginski A I. The SQUID Handbook. Weinheim: Wiley-VCH Verlag GmbH & Co. KGaA, 2004
67 Irwin K D, Nam S W, Cabrera B, et al. A self-biasing cryogenic particle detector utilizing electrothermal feedback and a SQUID readout. IEEE Trans Appl Supercond, 1995, 5: 2690–2693
68 Irwin K. An application of electrothermal feedback for high resolution cryogenic particle detection. Appl Phys Lett, 1995, 66: 1998–2000
69 Chervenak J A, Irwin K D, Grossman E N, et al. Superconducting multiplexer for arrays of transition edge sensors. Appl Phys Lett, 1999, 74: 4043–4045
70 Chervenak J A, Grossman E N, Irwin K D, et al. Performance of multiplexed SQUID readout for cryogenic sensor arrays. Nucl Instruments Methods Phys Res Sect A-Accelerators Spectrometers Detectors Associated Equipment, 2000, 444: 107–110
71 Benford D, Allen C, Chervenak J, et al. Multiplexed readout of superconducting bolometers. Int J Infrared Millimeter Waves, 2000, 21: 1909–1916
72 Doriese W B, Ullom J N, Beall J A, et al. 14-pixel, multiplexed array of gamma-ray microcalorimeters with 47 eV energy resolution at 103 keV. Appl Phys Lett, 2007, 90: 193508
73 Woodcraft A L, Ade P A R, Bintley D, et al. Electrical and optical measurements on the first SCUBA-2 prototype 1280 pixel submillimeter superconducting bolometer array. Rev Sci Instruments, 2007, 78: 024502
74 de Korte P A J, Beyer J, Deiker S, et al. Time-division superconducting quantum interference device multiplexer for transition-edge sensors. Rev Sci Instruments, 2003, 74: 3807–3815
75 Cunningham M, Ullom J, Miyazaki T, et al. High-resolution operation of frequency-multiplexed transition-edge photon sensors. Appl Phys Lett, 2002, 81: 159–161
76 Yoon J, Clarke J, Gildemeister J M, et al. Single superconducting quantum interference device multiplexer for arrays of low-temperature sensors. Appl Phys Lett, 2001, 78: 371–373
77 Oxley P, Ade P A, Baccigalupi C, et al. The EBEX experiment. In: Proceedings of SPIE, 2004. 5543: 320–331
78 Ruhl J, Ade P A, Carlstrom J E, et al. The south pole telescope. In: Proceedings of SPIE, 2004. 5498: 11–29
79 Dobbs M, Halverson N W, Ade P A R, et al. APEX-SZ first light and instrument status. New Astron Rev, 2006, 50: 960–968
80 Niemack M D, Beyer J, Cho H M, et al. Code-division SQUID multiplexing. Appl Phys Lett, 2010, 96: 163509
81 Bennett D A, Mates J A, Gard J D, et al. Integration of TES microcalorimeters with microwave SQUID multiplexed readout. IEEE Trans Appl Superconduct, 2014, 25: 1–5
82 Irwin K D, Lehnert K W. Microwave SQUID multiplexer. Appl Phys Lett, 2004, 85: 2107–2109
83 Mates J A B, Becker D T, Bennett D A, et al. Simultaneous readout of 128 X-ray and gamma-ray transition-edge microcalorimeters using microwave SQUID multiplexing. Appl Phys Lett, 2017, 111: 062601

84 Stanchfield S M, Ade P A R, Aguirre J, et al. Development of a microwave SQUID-multiplexed TES array for MUSTANG-2. J Low Temp Phys, 2016, 184: 460–465
85 Smith S J, Adams J S, Bailey C N, et al. Small pitch transition-edge sensors with broadband high spectral resolution for solar physics. J Low Temp Phys, 2012, 167: 168–175
86 Eckart M, Adams J, Bandler S, et al. Large-absorber TES X-ray microcalorimeters and the micro-X detector array. In: AIP Conference Proceedings, 2009. 1185: 699–702
87 Morgan K M, Pappas C G, Bennett D A, et al. Dependence of transition width on current and critical current in transition-edge sensors. Appl Phys Lett, 2017, 110: 212602
88 Hays-Wehle J P, Schmidt D R, Ullom J N, et al. Thermal conductance engineering for high-speed TES microcalorimeters. J Low Temp Phys, 2016, 184: 492–497
89 Wollman D A, Nam S W, Newbury D E, et al. Superconducting transition-edge-microcalorimeter X-ray spectrometer with 2 eV energy resolution at 1.5 keV. Nucl Instruments Methods Phys Res Sect A-Accelerators Spectrometers Detectors Associated Equipment, 2000, 444: 145–150
90 Wood G H, White B L. Pulses induced in tunneling currents between superconductors by alpha-particle bombardment. Appl Phys Lett, 1969, 15: 237–239
91 Peacock A, Verhoeve P, Rando N, et al. Single optical photon detection with a superconducting tunnel junction. Nature, 1996, 381: 135–137
92 Kozin M G, Romashkina I L, Sergeev S A, et al. STJ X-ray detectors with titanium sublayer. Nucl Instruments Methods Phys Res Sect A-Accelerators Spectrometers Detectors Associated Equipment, 2004, 520: 250–253
93 Twerenbold D. Nonequilibrium model of the superconducting tunneling junction X-ray detector. Phys Rev B, 1986, 34: 7748–7759
94 Gray K E. A superconducting transistor. Appl Phys Lett, 1978, 32: 392–395
95 Lerch P, Zehnder A. Quantum Giaever detectors: STJ's. In: Cryogenic Particle Detection. Berlin: Springer, 2005. 217–266
96 Angloher G, Hettl P, Huber M, et al. Energy resolution of 12 eV at 5.9 keV from Al-superconducting tunnel junction detectors. J Appl Phys, 2001, 89: 1425–1429
97 Ukibe M, Fujii G, Shiki S, et al. Modification of layer structures of superconducting tunnel junctions to improve X-ray energy resolution. J Low Temp Phys, 2016, 184: 200–205
98 Doyle S, Naylon J, Cox J, et al. Kinetic inductance detectors for 200 μm astronomy. In: Proceedings of SPIE, 2006. 6275: 62751O
99 Doyle S, Mauskopf P, Naylon J, et al. Lumped element kinetic inductance detectors. J Low Temp Phys, 2008, 151: 530–536
100 Yang C, Niu R R, Guo Z S, et al. Lumped element kinetic inductance detectors based on two-gap MgB_2 thin films. Appl Phys Lett, 2018, 112: 022601
101 Nam S B. Theory of electromagnetic properties of superconducting and normal systems. I. Phys Rev, 1967, 156: 470–486
102 Day P K, Leduc H G, Goldin A, et al. Antenna-coupled microwave kinetic inductance detectors. Nucl Instruments Methods Phys Res Sect A-Accelerators Spectrometers Detectors Associated Equipment, 2006, 559: 561–563
103 Doyle S, Mauskopf P, Naylon J, et al. Lumped element kinetic inductance detectors. J Low Temp Phys, 2008, 151: 530–536
104 Rösch M. Development of Lumped Element Kinetic Inductance Detectors for mm-wave Astronomy at the IRAM 30 m Telescope. Karlsruhe: KIT Scientific Publishing, 2014
105 Bueno J, Murugesan V, Karatsu K, et al. Ultrasensitive kilo-pixel imaging array of photon noise-limited kinetic inductance detectors over an octave of bandwidth for THz astronomy. J Low Temp Phys, 2018, 193: 96–102
106 Zobrist N, Daal M, Corbin J Y, et al. Disk resonator design for kinetic inductance detectors. J Low Temp Phys, 2019, 194: 394–403
107 O'Connell A D, Ansmann M, Bialczak R C, et al. Microwave dielectric loss at single photon energies and millikelvin temperatures. Appl Phys Lett, 2008, 92: 112903
108 Baselmans J, Yates S J C, Barends R, et al. Noise and sensitivity of aluminum kinetic inductance detectors for sub-mm astronomy. J Low Temp Phys, 2008, 151: 524–529
109 Gao J, Zmuidzinas J, Mazin B A, et al. Noise properties of superconducting coplanar waveguide microwave resonators. Appl Phys Lett, 2007, 90: 102507
110 Marsili F, Najafi F, Dauler E, et al. Single-photon detectors based on ultranarrow superconducting nanowires. Nano Lett, 2011, 11: 2048–2053
111 Caloz M, Perrenoud M, Autebert C, et al. High-detection efficiency and low-timing jitter with amorphous superconducting nanowire single-photon detectors. Appl Phys Lett, 2018, 112: 061103
112 Yang J K W, Kerman A J, Dauler E A, et al. Modeling the electrical and thermal response of superconducting nanowire single-photon detectors. IEEE Trans Appl Supercond, 2007, 17: 581–585

113 Semenov A D, Gol'tsman G N, Korneev A A. Quantum detection by current carrying superconducting film. Phys C-Supercond, 2001, 351: 349–356
114 Natarajan C M, Tanner M G, Hadfield R H. Superconducting nanowire single-photon detectors: physics and applications. Supercond Sci Technol, 2012, 25: 063001
115 Renema J J, Gaudio R, Wang Q, et al. Experimental test of theories of the detection mechanism in a nanowire superconducting single photon detector. Phys Rev Lett, 2014, 112: 117604
116 Eisaman M D, Fan J, Migdall A, et al. Invited review article: single-photon sources and detectors. Rev Sci Instrum, 2011, 82: 071101
117 Semenov A, Engel A, Hübers H W, et al. Spectral cut-off in the efficiency of the resistive state formation caused by absorption of a single-photon in current-carrying superconducting nano-strips. Eur Phys J B, 2005, 47: 495–501
118 Zotova A N, Vodolazov D Y. Photon detection by current-carrying superconducting film: a time-dependent Ginzburg-Landau approach. Phys Rev B, 2012, 85: 024509
119 Bulaevskii L N, Graf M J, Batista C D, et al. Vortex-induced dissipation in narrow current-biased thin-film superconducting strips. Phys Rev B, 2011, 83: 144526
120 Becker W. Advanced Time-Correlated Single Photon Counting Techniques. Berlin: Springer, 2005
121 Zhang X. Characteristics of tungsten silicide and its application for single X-ray photon detection. Dissertation for Ph.D. Degree. Zurich: University of Zurich, 2018